doi:10.1093/brain/awx272 BRAIN 2017: Page 1 of 17 | 1

BRAIN
A JOURNAL OF NEUROLOGY

Epigenetic editing of the *Dlg4*/PSD95 gene improves cognition in aged and Alzheimer's disease mice

Fernando J. Bustos,[1,2] Estibaliz Ampuero,[1] Nur Jury,[1] Rodrigo Aguilar,[1,2] Fahimeh Falahi,[3] Jorge Toledo,[4,5] Juan Ahumada,[6] Jaclyn Lata,[7] Paula Cubillos,[1] Berta Henríquez,[1,*] Miguel V. Guerra,[1] Jimmy Stehberg,[1] Rachael L. Neve,[8,#] Nibaldo C. Inestrosa,[9] Ursula Wyneken,[10] Marco Fuenzalida,[6] Steffen Härtel,[4,5] Miguel Sena-Esteves,[7] Lorena Varela-Nallar,[1] Marianne G. Rots,[3,$] Martin Montecino[1,2,$] and Brigitte van Zundert[1,$]

[$]These authors contributed equally to this work.

The *Dlg4* gene encodes for post-synaptic density protein 95 (PSD95), a major synaptic protein that clusters glutamate receptors and is critical for plasticity. PSD95 levels are diminished in ageing and neurodegenerative disorders, including Alzheimer's disease and Huntington's disease. The epigenetic mechanisms that (dys)regulate transcription of *Dlg4*/PSD95, or other plasticity genes, are largely unknown, limiting the development of targeted epigenome therapy. We analysed the *Dlg4*/PSD95 epigenetic landscape in hippocampal tissue and designed a *Dlg4*/PSD95 gene-targeting strategy: a *Dlg4*/PSD95 zinc finger DNA-binding domain was engineered and fused to effector domains to either repress (G9a, Suvdel76, SKD) or activate (VP64) transcription, generating artificial transcription factors or epigenetic editors (methylating H3K9). These epi-editors altered critical histone marks and subsequently *Dlg4*/PSD95 expression, which, importantly, impacted several hippocampal neuron plasticity processes. Intriguingly, transduction of the artificial transcription factor PSD95-VP64 rescued memory deficits in aged and Alzheimer's disease mice. Conclusively, this work validates PSD95 as a key player in memory and establishes epigenetic editing as a potential therapy to treat human neurological disorders.

1 Center for Biomedical Research, Faculty of Biological Sciences and Faculty of Medicine, Universidad Andres Bello, Avenida Republica 217, Santiago, Chile
2 FONDAP Center for Genome Regulation, Chile
3 University of Groningen, University Medical Center Groningen, Groningen, The Netherlands
4 Anatomy and Developmental Biology, SCIAN-Lab, Institute of Biomedical Sciences, Biomedical Neuroscience Institute, Center for Medical Informatics and Telemedicine CIMT, National Center for Health Information Systems CENS, Santiago, Chile
5 Faculty of Medicine, Universidad de Chile, Santiago, Chile
6 Centro de Neurobiología y Plasticidad Cerebral, Departamento de Fisiología, Facultad de Ciencias, Universidad Valparaíso, Chile
7 Department of Neurology and Horae Gene Therapy Center, University of Massachusetts Medical School, Worcester, MA, USA
8 Department of Brain and Cognitive Sciences, Massachusetts Institute of Technology, Cambridge, Massachusetts, USA
9 CARE Biomedical Research Center, Faculty of Biological Sciences, Pontificia Universidad Católica de Chile, Chile
10 Laboratorio de Neurociencias, Universidad de Los Andes, Santiago, Chile

[*]Present address: Faculty of Science, Universidad San Sebastian, Santiago, Chile
[#]Present address: Gene Delivery Technology Core at Massachusetts General Hospital, Cambridge, Massachusetts, USA

Correspondence to: Brigitte van Zundert
Center for Biomedical Research, Faculty of Biological Sciences and Faculty of Medicine, Universidad Andres Bello, Santiago, Chile
E-mail: bvanzundert@unab.cl

Received April 24, 2017. Revised August 16, 2017. Accepted August 27, 2017.

Correspondence may also be addressed to:
Martin Montecino
E-mail: mmontecino@unab.cl
Marianne G. Rots
University of Groningen, University Medical Center Groningen, Groningen, The Netherlands
E-mail: m.g.rots@umcg.nl

Keywords: ATF; ZFP; PSD-95; epigenetics; Alzheimer's disease

Abbreviations: ATF = artificial transcription factor; AAV = adeno-associated virus; ChIP = chromatin immunoprecipitation; HSV = herpes simplex virus; NOR = novel object recognition; OLM = object location memory; SKD = super Krüppel-associated box (KRAB) domain; ZFP = zinc finger protein

Introduction

Epigenetic modifications of histone tails, including acetylation and methylation, play an essential role in gene transcription (Bannister and Kouzarides, 2011; Gardner *et al.*, 2011). As such, epigenetic regulation serves key roles in the development, differentiation, maintenance and survival of diverse brain cells, hence impacting neuronal plasticity and memory (Gräff and Tsai, 2013; Sweatt, 2013). While epigenetic dysregulation is implicated in several neurodevelopmental, neuropsychiatric and neurodegenerative disorders, including Alzheimer's and Huntington's diseases (Gräff *et al.*, 2011; Dekker *et al.*, 2014; Frost *et al.*, 2014), it is challenging to directly associate epigenetic (dys)regulation with specific neuronal or behavioural phenotypes.

To facilitate studies on the biological roles of chromatin modifications, genome modification technologies have been further developed to allow targeted overwriting of the epigenetic signature at endogenous loci, known as epigenetic editing (de Groote *et al.*, 2012; Voigt and Reinberg, 2013; Stricker *et al.*, 2017). Programmable DNA binding platforms, including zinc finger proteins (ZFPs), transcription activation-like effectors (TALE), and more recently clustered regularly interspaced short palindromic repeats (CRISPR), have been exploited to induce locus-specific epigenetic editing by fusing these DNA binding domains targeting an endogenous locus to minimal effector domains of chromatin-modifying enzymes (Gaj *et al.*, 2013). Such epigenome editing tools (epi-editors) have been used to manipulate gene expression in several *in vitro* studies (Falahi *et al.*, 2013; Konermann *et al.*, 2013; Mendenhall *et al.*, 2013; Chen *et al.*, 2014; Hilton *et al.*, 2015; Cano-Rodriguez *et al.*, 2016). Moreover, recent studies show that *in vivo* genome editing improves muscle function in mouse models of Duchenne muscular dystrophy (Long *et al.*, 2016; Nelson *et al.*, 2016; Tabebordbar *et al.*, 2016). So far, limited studies have investigated epigenetic editing in the CNS. Specifically, viral-mediated delivery of six-fingered ZFPs targeting the immediate early gene *FosB* (Heller *et al.*, 2014) or the cyclin-dependent kinase 5 gene (*Cdk5*) (Heller *et al.*, 2016) in the mouse brain reward region nucleus accumbens was shown to regulate addiction- and depression-related behavioural responses. In these studies, the *FosB*-ZFPs and *CDK5*-ZFPs were fused to the histone methyltransferase enzyme G9a to induce targeted di-methylation of histone H3 lysine 9 (H3K9me2), a mark associated with transcriptional repression (Shankar *et al.*, 2013). Six-fingered ZFPs are the most advanced engineered DNA-binding domains, and several ongoing clinical trials have not demonstrated adverse effects (Gaj *et al.*, 2013; Falahi *et al.*, 2015). In addition to epi-editors, artificial transcription factors (ATFs) have been used to alter transcription in the brain (Laganiere *et al.*, 2010; Konermann *et al.*, 2013; Heller *et al.*, 2014, 2016). For ATFs, fusion of the non-catalytic transactivation domain of the viral protein VP16, or of its tetramer (VP64), to DNA binding domains strongly promotes transcriptional activation, whereas fusion of the super Krüppel-associated box (KRAB) domain (SKD) induces robust transcriptional silencing. How ATFs regulate gene expression is not fully understood, but their lack of intrinsic catalytic activity suggests that they function transiently, by recruiting other proteins such as histone-modifying enzymes to alter gene transcription (Beltran and Blancafort, 2011; de Groote *et al.*, 2012; Huisman *et al.*, 2013).

There is an urgent need to elucidate how epigenetic processes regulate the expression of key neuron-related protein coding genes involved in fundamental neurological processes such as neuronal plasticity and memory. A master regulator involved in these processes is the postsynaptic density protein 95 (PSD95), transcribed from the gene discs large homolog 4 (*Dlg4*). PSD95 is the most abundant scaffolding protein in the excitatory postsynaptic density, interacting and regulating a large number of important molecules for neuronal function such as synaptic glutamate receptors, signalling proteins, adhesion molecules, cytoskeletal proteins, and other scaffolding proteins (van Zundert *et al.*, 2004; Elias and Nicoll, 2007). We and others have used conventional gain (cDNA) and loss (RNAi) of function approaches to show that PSD95 plays a critical role in organizing the postsynaptic synapse, thereby limiting plasticity and hence stabilizing the neuronal circuitry (El-Husseini *et al.*, 2000; Losi *et al.*, 2003; Charych *et al.*, 2006; Ehrlich *et al.*, 2007; Elias *et al.*, 2008; Henriquez *et al.*, 2013; Bustos *et al.*, 2014). Moreover, it has been reported that the expression of PSD95 is aberrant in several

human disorders that affect the central and peripheral nervous systems, including in Alzheimer's disease, Huntington's disease, schizophrenia, autism spectrum disorders, and pain disorders (Arbuckle *et al.*, 2010; de Bartolomeis *et al.*, 2014; Savioz *et al.*, 2014; Zhang *et al.*, 2014; Hong *et al.*, 2016).

Targeted *Dlg4*/PSD95 gene knock-down by RNAi-based approaches could be used in human gene therapies; however, these approaches are not ideal for treating patients suffering chronic brain diseases as the large amounts of RNA required can induce toxicity and moreover their effects are only temporary (Kanasty *et al.*, 2012). These limitations can be overcome by epigenetic editing of the *Dlg4*/PSD95 locus. Here we elucidated key epigenetic mechanisms that control *Dlg4*/PSD95 gene expression during rat hippocampus development. This information, together with the use of genome editing technologies, allowed us to epigenetically reprogram the *Dlg4*/PSD95 promoter. Such epigenetic editing controlled gene expression both *in vitro* and *in vivo*, influencing function and structure of neurons as well as recognition memory in aged mice and in a mouse model of Alzheimer's disease (AβPPswe/PS-1).

Materials and methods

For detailed materials and methods please refer to the Supplementary material.

Animals

All protocols involving rodents were carried out according to NIH and ARRIVE guidelines, and were approved by the Ethical and Bio-security Committees of Universidad Andrés Bello. Wild-type rats (Sprague-Dawley), wild-type mice and AβPPswe/PS-1 mice (004462 from Jackson laboratory) were used.

Chromatin immunoprecipitation assays

Chromatin immunoprecipitation (ChIP) assays were used on hippocampal tissue as described (Henriquez *et al.*, 2013). Briefly, rat hippocampi were double cross-linked, homogenized, and sheared in a water bath sonicator Bioruptor (Diagenode Inc.) to obtain fragments of 500 bp or smaller. Chromatin was immunoprecipitated with specific antibodies recognizing histone post-translational modifications and chromatin-modifying enzymes. Immuno-complexes were recovered with protein A or G agarose beads and DNA was recovered by phenol/chloroform extraction and ethanol precipitation. Quantitative PCR was performed with specific primers for the *Dlg4*/PSD95 promoter region, *Dlg4*/PSD95 coding region, or *Runx2* P1 promoter region.

Chromatin immunoprecipitation sequencing

Precipitated DNA obtained from ChIP experiments was used to construct libraries, and sequenced using pair-end reads for 300 cycles on a MiSeq™ desktop sequencer (Illumina). Sequences were aligned with Bowtie2 (Langmead and Salzberg, 2012) against the latest *Rattus norvegicus* genome (rn4) and peak detection was performed using Avadis NGS software (Strand).

Bisulfite sequencing

Sequencing of methylated DNA sequences was performed as described (Falahi *et al.*, 2013; Huisman *et al.*, 2013). Methylation status of 12 CpGs in the *Dlg4*/PSD95 DNA promoter sequence was determined by bisulfite sequencing. Genomic DNA was obtained from hippocampal tissue, using the Quick-gDNA™ kit (Zymo Research), following manufacturer's instructions. Genomic DNA was bisulfite-converted with the EZ DNA Methylation-Gold™ (Zymo Research) kit. The region was amplified using specific primers and cloned into pCR2.1 vector (Life technologies) for sequencing.

Engineering of PSD95-6ZF constructs

Dlg4/PSD95 gene promoter sequence was analysed using databases for transcription start sites. The region between −200 and +100 was screened for putative zinc finger proteins (ZFPs) that comprise 6 zinc fingers fused together (6ZFP) to enable targeting 18 contiguous base pairs (www.zincfinger-tools.org) (Mandell and Barbas, 2006). ZFPs with high affinity and target site specificity were selected. The following zinc fingers with high affinity and target site specificity were selected to target the *Dlg4*/PSD95 promoter DNA sequence: 3′-GAATGAGGGGAGGGGAGG-5′. The resulting amino acid sequence of the complete PSD95-6ZF is as follows: LEPGEKPYKCPECGKSFSQSSNLVRHQRTHTGEKPYKCPECGKSFSQAGHLASHQRTHTGEKPYKCPECGKSFSRSDKLVRHQRTHTGEKPYKCPECGKSFSRSDNLVRHQRTHTGEKPYKCPECGKSFSRSDKLVRHQRTHTGEKPYKCPECGKSFSRSDHLTNHQRTHTGKKTS. The helices that interact with the DNA sequence are underlined. For expression, the construct was subcloned into a pMX-IRES-GFP retroviral vector containing the transcription effector domains VP64, SKD, and the sequence of catalytic domains of the histone methyltransferase enzymes G9a and Suvdel76 (Falahi *et al.*, 2013). To infect primary hippocampal neurons, all PSD95-6ZF-fusion constructs were subcloned into a lentiviral bicistronic pCDH vector expressing cop-GFP (System Biosciences) and lentiviral particles produced. To infect neurons *in vivo*, PSD95-6ZF-fusion constructs were subcloned into p1005 herpes simplex virus (HSV) vector, or into adeno-associated virus (AAV) vectors to produce viral particles. All vectors used for HSV, AAV, retroviral and lentiviral production coded for the expression of GFP using an independent promoter.

Viral particles

Lentiviral particles were prepared as described (Henriquez *et al.*, 2013). To produce retroviral and lentiviral vectors,

HEK293FT cells were grown in 100 mm culture plates to 80–90% confluence; Lipofectamine™ 2000 reagent (Life Technologies; following manufacturer's instructions) or $CaPO_4$ was used to transfect cells with the pMX or pCDH plasmid containing the PSD95-6ZFP and effector domains (VP64, SKD, G9a, or Suvdel76), together with viral packaging plasmids (containing cDNA encoding gag-pol and the vesicular stomatitis virus G protein). Empty pMX or pCDH plasmids (GFP only), and backbones with only PSD95-6ZFPs, were used as control. Also, we made use of HSV viruses (3×10^8 transducing units/ml) expressing GFP alone, or together with PSD95-6ZFP-Suvdel76 or PSD95-6ZFP-VP64. GFP expression in HSVs is driven by a CMV promoter, whereas the gene of interest is driven by an IE4/5 promoter (Neve *et al.*, 2005; van Zundert *et al.*, 2008; Heller *et al.*, 2014). To allow for an efficient, widespread and long-term transduction of the constructs in the brain, AAV vectors were used. AAV vectors encoding ATFs under a chicken β-actin (CBA) promoter also carried an IRES-GFP cassette. AAV-PHP.B vectors were produced by transient transfection of HEK293 cells followed by purification using iodixanol gradient centrifugation. The AAV-PHP.B capsid gene was synthesized based on the published sequence (Genbank KU056473; Deverman *et al.*, 2016) and cloned in a trans-complementing plasmid carrying the AAV2 Rep gene as previously described (Broekman *et al.*, 2006).

Stereotaxic injections

Bilateral hippocampal stereotaxic injections of viral particles were performed as previously described for HSV particles (Ampuero *et al.*, 2017; Bustos *et al.*, 2017). Briefly, adult mice were anaesthetized with saline (5 µl saline/gram body weight) containing 170 mg/kg ketamine plus 17 mg/kg xylazine. For spine morphology analysis, 1.0 µl of 10% diluted HSV (0.1 µl of $\sim 10^8$ infectious units/ml + 0.9 µl HEPES) was injected into dentate gyrus, with the following coordinates: ±1.5 mm lateral; −2 mm anteroposterior; −2.3 mm ventral from bregma (Tashiro *et al.*, 2006). For hippocampal electrophysiology recordings, 1.0 µl of 25% diluted HSV (0.25 µl of $\sim 10^8$ infectious units/ml + 0.75 µl HEPES) was injected into dentate gyrus (±1.5 mm lateral; −2 mm anteroposterior; −2.3 mm ventral from bregma), CA1 (±1.5 mm lateral; −2 mm anteroposterior; −1.3 mm ventral from bregma) and CA3 (±2.5 mm lateral; −2 mm anteroposterior; −1.5 mm ventral from bregma (Tashiro *et al.*, 2006). For behavioural studies, HSVs (0.5 µl 25% diluted) or AAVs (0.5 µl undiluted) were bilaterally injected into CA1 and dentate gyrus using the above coordinates.

Spine morphology

Secondary dendrite shafts (⩾30 µm) were selected from granular neurons of the dentate gyrus and high magnification images were acquired with an UltraView RS spinning disk microscope (Perkin Elmer) with a 100× oil objective (NA = 1.3, C-Apochromat), excited with a 488 nm diode laser (Omicron), and captured with a 12-bit CCD camera (Hamamatsu ORCA-ER). Images were deconvolved, segmented and 3D reconstructions made. Total number of spines, spine density along the dendrite, and quantitative morphological descriptors were calculated from the 3D voxel models, as described earlier (Härtel *et al.*, 2007). Spine shapes were defined using the morphological descriptors as follows: (i) filopodia: length ⩾1.5 µm and entropy <0.91; (ii) mushroom: <1.5 µm in length and >0.45 µm in width; (iii) stubby: <1.5 µm in length, >0.45 relative volume and <0.5 µm in elongation; (iv) thin: <1.5 µm length and <0.45 in width or <1.5 µm in length and >0.5 in elongation.

Electrophysiology

Slice preparation and whole-cell electrophysiological recordings on single neurons were performed as previously described (Fuenzalida *et al.*, 2007; Vargas *et al.*, 2014). All recordings were made with picrotoxin (50 µM, Tocris) in the artificial CSF. The evoked excitatory postsynaptic current (eEPSC) was elicited by bipolar stimulation. The measurement of the NMDA/AMPA receptor ratio was performed similarly as previously described (Myme *et al.*, 2003; Ehrlich *et al.*, 2007).

Novel object recognition and object location memory tests

The single trail novel object recognition (NOR) and object location memory (OLM) tests consisted of three steps: habituation, a training session (10 min), test session (10 min) 24 h later. Mice were individually habituated in an apparatus that contained a cage inside an insonorized chamber. In the training session, the cage contained two identical objects, termed 'familiar objects' in NOR and 'non-displaced objects' in OLM. In the NOR test session, one familiar object (F) was replaced by a novel object (N). In the OLM test session, the location of one non-displaced object (non-D) was changed, termed displaced object (D). The exploration time was recorded and defined as time spent sniffing or touching the object with the nose and/or forepaws. For NOR, the 'recognition index' was calculated by the time spent to explore object N compared to total time explored in both objects (N + F). For OLM, the 'discrimination index' was calculated by the time spent to explore object D compared to total time explored in both objects (D + non-D).

Memory flexibility test

The memory flexibility task was performed as previously described (Serrano *et al.*, 2014) with slight modifications. The mice were trained in a circular water maze to find a circular platform of 10 cm localized at 1 cm below water level. Each animal was trained for one pseudo-random location of the platform per day for 4 days, with a new platform location each day. The maximum swimming trial duration was 60 s and animals were allowed to spend 10 s on the platform at the end of each trial. Up to 15 training trials were performed per day or until the animal met a criterion of three successive trials within an escape latency of <20 s.

Statistical analyses

One-way ANOVA followed by the Dunnett's *post hoc* was used to detect intervals, in which significant changes occurred, for all datasets where a parameter was measured

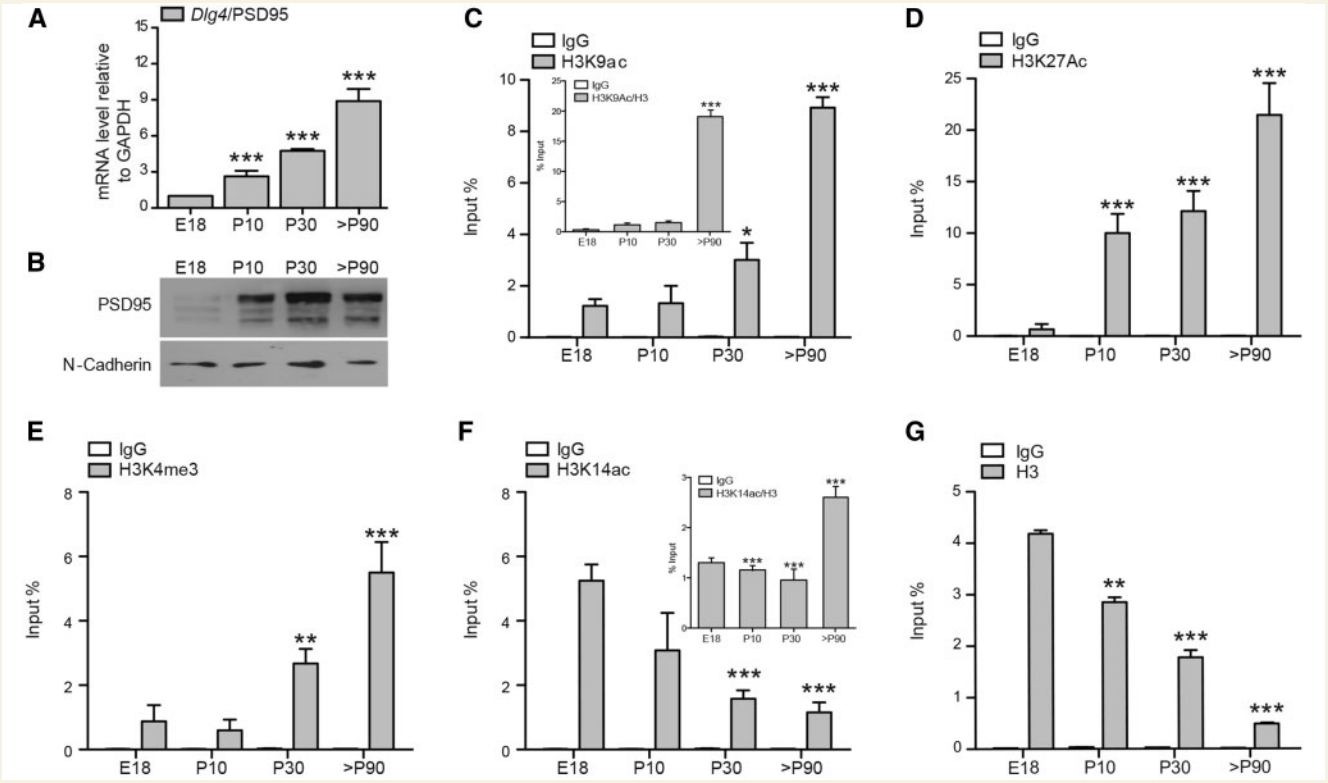

Figure 1 Concomitant with the upregulation of *Dlg4*/PSD95 gene expression during development, its promoter becomes enriched for active histone tail marks. (**A**) Total RNA was extracted from hippocampal tissues on E18, P10, P30 or ⩾P90, and *Dlg4*/PSD95 mRNA levels were quantified by qRT-PCR. Results were normalized against mRNA levels of *GAPDH*. E = embryonic day; P = postnatal day. (**B**) Levels of PSD95 protein were analysed by western blots of whole cell extracts from hippocampal tissues, using antibodies against PSD95 (N-cadherin served as loading control). (**C–G**) ChIP assays were performed on chromatin from hippocampal tissue at indicated developmental stages, using antibodies against (**C–F**) active histone tail modifications, or (**G**) histones in the following order: (**C**) H3K9ac, (**D**) H3K27ac, (**E**) H3K14ac, (**F**) H3K4me3, or (**G**) histone H3. Specific primers for the *Dlg4*/PSD95 gene promoter, encompassing the transcription start site (TSS), were used to quantify precipitated DNA by qPCR (see Fig. 4A). All results were normalized against input material; non-specific IgG served as control. Bars represent mean ± SEM from at least three independent experiments. Statistical analysis was performed using ANOVA test. $^{*}P < 0.05$, $^{**}P < 0.01$ and $^{***}P < 0.001$, relative to E18.

across time points following a specific treatment. Student's *t*-test was applied when two populations of responses were examined. For all figures, error bars represent the standard error of the mean (SEM); $^{*}P \leqslant 0.05$, $^{**}P \leqslant 0.01$, $^{***}P \leqslant 0.001$.

See Supplementary material for more details on the methods described above and on cell cultures, transfections and infections; qRT-PCR assays; western blot assays; synaptic membrane preparations; dendritic arbor analysis *in vitro*.

Results

Histone modification patterns at the *Dlg4*/PSD95 gene promoter in developing hippocampus

To gain understanding in the epigenetic mechanisms that control *Dlg4*/PSD95 gene expression in the maturing hippocampus, we first assessed *Dlg4*/PSD95 mRNA and protein levels. We observed a gradual increase in *Dlg4*/PSD95 mRNA and protein levels throughout the developing rat hippocampus [embryonic Day 18 (E18), and postnatal Days 10 (P10), 30 (P30) and ⩾90 (P90)], with highest levels found in adult hippocampus (Fig. 1A and B). Next, we investigated if this *Dlg4*/PSD95 expression pattern was related with an increase in active or a decrease in silencing epigenetic marks at the *Dlg4*/PSD95 promoter by using antibodies against specific histone H3 modifications to perform ChIP, followed by quantitative PCR (ChIP-qPCR) with primers for the *Dlg4*/PSD95 promoter (see model, Fig. 4A). We found that the increased expression was associated with gradual enrichment of the active marks H3K9ac (Fig. 1C), H3K27ac (Fig. 1D), H3K4me3 (Fig. 1E), but not H3K14ac (Fig. 1F; and see below) at the proximal *Dlg4*/PSD95 gene promoter. Levels of H3 (Fig. 1G) and H4 (not shown) gradually decreased throughout development, indicating that enhanced *Dlg4*/PSD95 gene expression was accompanied by progressive nucleosome

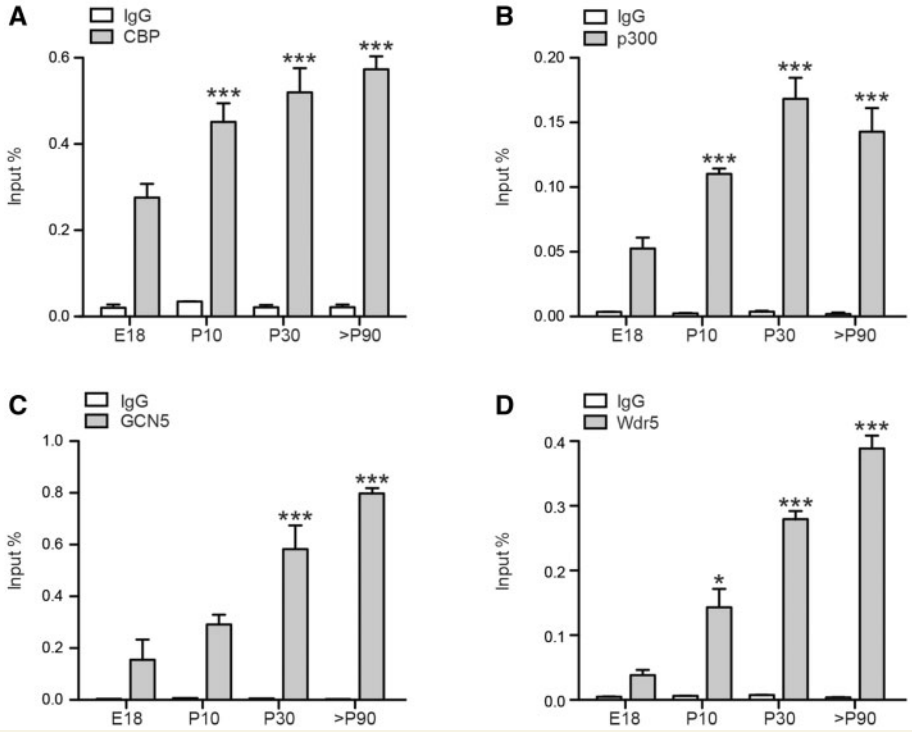

Figure 2 Enrichment of active histone tail marks at the *Dlg4*/PSD95 gene promoter occurs in parallel with increased binding of chromatin-modifying enzymes at this site. (**A–D**) ChIP assays were performed on chromatin prepared from hippocampal tissue at the indicated developmental stages, using antibodies against the chromatin-modifying enzymes (**A**) CBP, (**B**) p300, (**C**) GCN5, or (**D**) Wdr5. *Dlg4*/PSD95 primers were used for qPCR. Results were normalized against input material and non-specific IgG served as control. Bars represent means ± SEM from at least three independent experiments. Statistical analysis was performed using ANOVA test. $^{*}P < 0.05$, $^{**}P < 0.01$ and $^{***}P < 0.001$, relative to E18.

depletion. Based on these findings we also analysed the data after normalizing for the amount of histones associated with *Dlg4*/PSD95 promoter region and observing that H3K9ac (Fig. 1C), H3K27ac (not shown) and H3K4me3 (not shown) were significantly higher enriched throughout hippocampal development, while the H3K14ac mark remained unchanged from E18-P30, and significantly increased >P90 (inset Fig. 1F). To complement the results of acetylated active marks, we examined the enrichment of three histone acetyltransferases, CREB-binding protein (CBP) (Fig. 2A), p300 (Fig. 2B), and GCN5 (Fig. 2C). All of them were gradually enriched at the *Dlg4*/PSD95 gene promoter with hippocampal maturation. The developmental enrichment of the active mark H3K4me3 at the *Dlg4*/PSD95 promoter (Fig. 1F) was accompanied by increased association of the critical component of its writer complex Wdr5 (Fig. 2D).

Next, we analysed the presence of transcriptional silencing marks. H3K9me2 and H3K9me3 were not detected at the *Dlg4*/PSD95 gene promoter throughout hippocampal development (Fig. 3A and B; grey bars). In contrast, these marks were observed for the *Dlg4*/PSD95 gene promoter in the myoblastic cell-line C2C12 (Fig. 3A and B; black bars), where this gene is not actively transcribed (Fig. 3F). We also found that G9a (Fig. 3C) and Suv39H1 (Fig. 3D)—two histone methyltransferase enzymes that di- and tri-methylate H3K9, respectively (Shankar *et al.*, 2013)—were highly associated with the *Dlg4*/PSD95 gene promoter in the myoblastic cell-line C2C12 (Fig. 3C and D; black bars), while their binding was not detected at this site in hippocampal tissue (Fig. 3C and D; grey bars). DNA methylation of CpG nucleotides in promoter regions is another important epigenetic mechanism used to silence gene transcription (Cedar and Bergman, 2012). Bisulfite sequencing analysis revealed that of the 12 CpGs present in the *Dlg4*/PSD95 proximal gene promoter region within the first ~400 bp upstream of transcription start sites (Zhang *et al.*, 2003), none were methylated in the hippocampus at any developmental stage tested (Fig. 3E; white circles), while two CpG sites were methylated in the myoblastic cell line C2C12 (Fig. 3E; black circles).

Altogether our results show that increased expression of *Dlg4*/PSD95 in the maturing rat hippocampus is accompanied by the gradual enrichment of active histone marks. Unexpectedly, neither typical repressive histone H3K9me2/3 marks nor DNA methylation were detected at the proximal *Dlg4*/PSD95 gene promoter in hippocampal cells, not even at early developmental stages when *Dlg4*/PSD95 expression is very low.

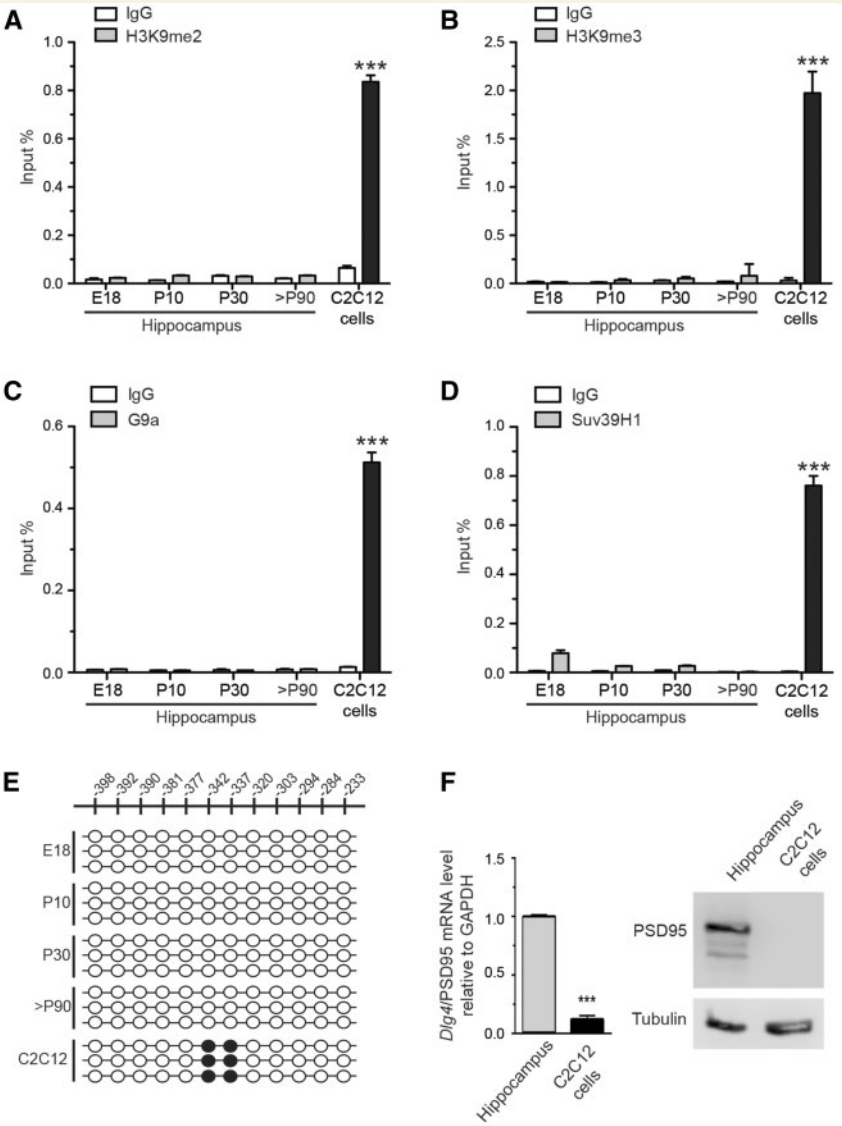

Figure 3 Typical repressive histone tail marks and DNA methylation are not detected at the *Dlg4*/PSD95 gene promoter in the developing hippocampus. (**A–D**) ChIP assays were performed on chromatin prepared from hippocampal tissue (grey bars) on E18, P10, P30 or ⩾P90; antibodies used were against the repressive marks (**A**) H3K9me2, (**B**) H3K9me3, or against the chromatin modifying enzymes (**C**) G9a, or (**D**) Suv39H1. Chromatin extracts from C2C12 cells (black bars) served as positive controls. *Dlg4*/PSD95 primers were used for qPCR. Results were normalized against input material; non-specific IgG served as control (white bars). Bars represent means ± SEM from at least three independent experiments. Statistical analysis was performed using ANOVA test. ***$P < 0.001$, relative to IgG for C2C12 cells. (**E**) Genomic DNA from developing hippocampi and C2C12 cells was extracted to perform bisulfite sequencing analysis on the 12 CpG sites located upstream of the *Dlg4*/PSD95 transcription start sites; unmethylated (open circles) versus methylated (closed circles). Each row represents the analysis of a single clone. (**F**) Total *Dlg4*/PSD95 mRNA and protein levels were measured by qRT-PCR (*left*) or western blot (*right*), respectively.

Design of a 6ZF construct that specifically targets the *Dlg4*/PSD95 gene promoter

Next, we explored an epigenetic editing strategy to control specifically the *Dlg4*/PSD95 transcriptional status in hippocampal neurons. We sought to induce the recruitment of chromatin-modifying enzymes to the *Dlg4*/PSD95 gene promoter capable of overwriting the original chromatin signature. Particularly, we engineered a DNA module containing six Cys2His2 zinc fingers (6ZF) to target an 18-bp sequence located in the proximal *Dlg4*/PSD95 promoter region (−38 to −21), upstream of the transcription start sites (Fig. 4A); the length of this sequence should theoretically provide unique sequence specificity (Gaj *et al.*, 2013; Falahi *et al.*, 2015). We incorporated also a haemagglutinin (HA)-tag and a nuclear localization signal into the PSD95-6ZF. Then, to determine whether the engineered DNA-binding zinc-finger motif effectively targeted the *Dlg4*/PSD95 gene promoter sequence, cultured rat hippocampal neurons were

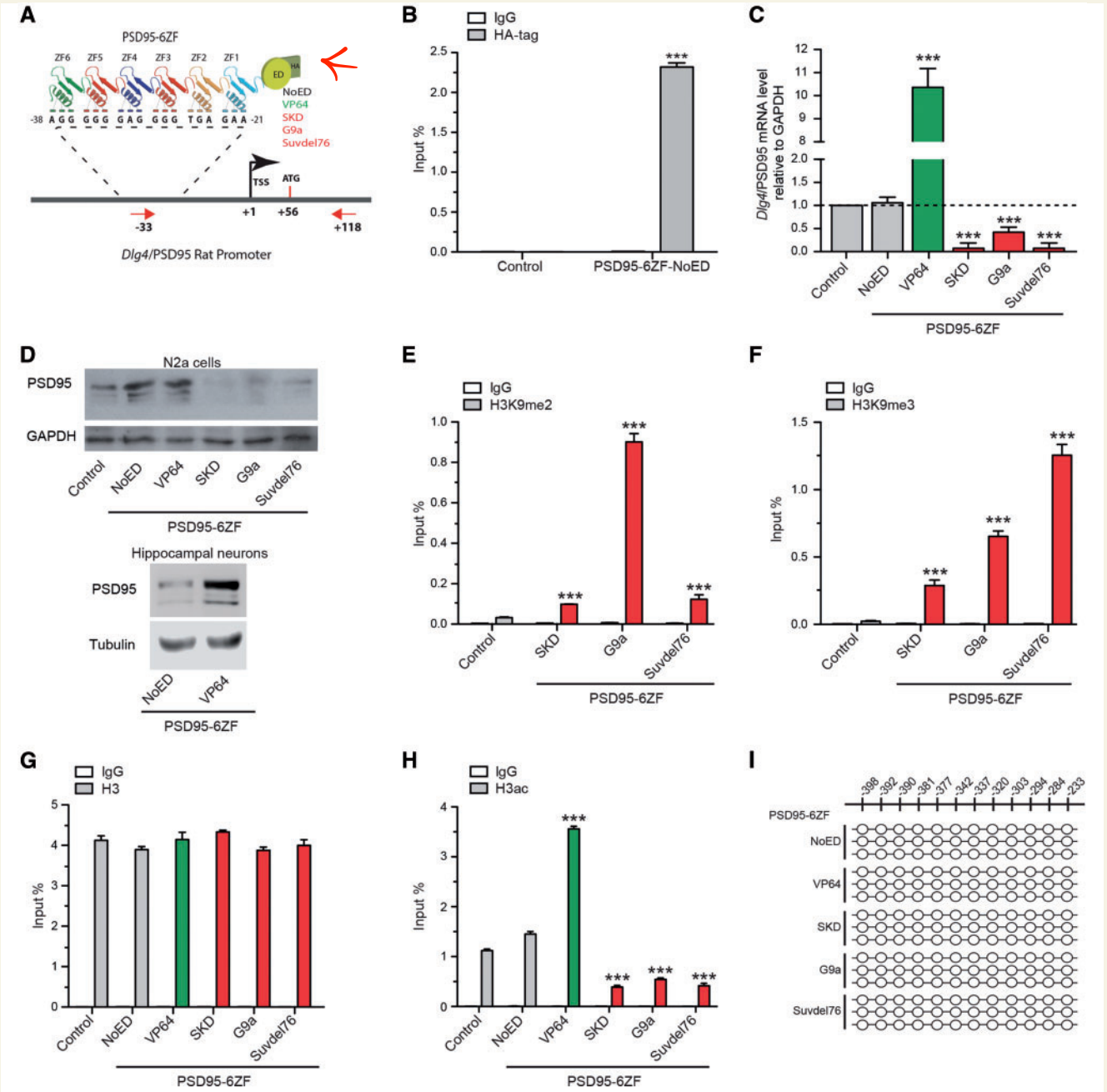

Figure 4 Engineered ZFPs and ATFs bidirectionally modulate *Dlg4*/PSD95 gene expression by altering histone post-translational modifications associated with the *Dlg4*/PSD95 promoter. (**A**) Schematic of the designed ZFPs and ATFs, and their binding to the *Dlg4*/PSD95 gene promoter relative to ATG and transcription start sites. ZF1 of the 6ZF DNA module is linked to haemagglutinin (HA). PSD95-6ZF-NoED refers to PSD95-6ZF not linked to any effector domain (ED). The PSD95-6ZF construct is fused to diverse effector domains to generate PSD95-6ZF-VP64, PSD95-6ZF-SKD, PSD95-6ZF-G9a or PSD95-6ZF-Suvdel76. The colour coding designed to the diverse constructs refers to gene transcription: black (neutral), green (activation) and red (repression). Red arrows indicate primers used to quantify the ChIP assays by qPCR. (**B**) Hippocampal neurons (*in vitro* Day 7) were infected with lentiviral vectors coding for GFP (Control) or PSD95-6ZF-NoED; at *in vitro* Day 12, ChIP assays were performed using an HA antibody (grey bar). Results were normalized against input material, and non-specific IgG served as a control (white bar). See also Supplementary Figs 1 and 2 for ChIP-seq. (**C–I**) N2a cells were infected for 72 h with the diverse constructs, as depicted. Total *Dlg4*/PSD95 mRNA and protein levels were measured by (**C**) qRT-PCR or by (**D**) western blot (*top*, N2a cells; *bottom*, hippocampal neurons), respectively. (**E–H**) ChIP-qPCR analyses using antibodies against (**E**) H3K9me2, (**F**) H3K9me3, (**G**) total histone H3, or (**H**) total histone H3 acetylation. Bars represent means ± SEM from three independent experiments, and statistical analysis was performed by (**B**) Student's *t*-test or (**C–H**) one-way ANOVA. ***$P < 0.001$, relative to control. (**I**) Bisulfite sequencing analysis performed on 12 CpG sites located in *Dlg4*/PSD95 promoter (as in Fig. 3E). See also Supplementary Fig. 3 for additional specificity of the 6ZF-fusion constructs.

transduced with a lentivirus vector encoding PSD95-6ZF-NoED (NoED, no effector domain). ChIP-qPCR assays revealed that PSD95-6ZF-NoED was strongly enriched at the *Dlg4*/PSD95 gene promoter (Fig. 4B). To confirm the specificity of PSD95-6ZF-NoED, we used whole-genome ChIP sequencing (ChIP-seq) technology. Genome-wide karyotype visualization of the ChIP-seq data showed that PSD95-6ZF-NoED was specifically and efficiently recruited to the chromosome 10q24 locus—where the *Dlg4*/PSD95 gene resides in rats (Supplementary Fig. 1)—with highest peaks (74 reads) mapped to the proximal promoter region of the *Dlg4*/PSD95 gene (chr10:56 861 701–56 863 601) (Supplementary Fig. 2A). As an internal control, we analysed samples exposed to an unrelated non-specific IgG (blue) and to input (green). Other sequences also showed some off-target binding of PSD95-6ZF-NoED, which were not associated with known promoter regions. The most significant of these was the rat Frizzled 1 (*Fzd1*) locus (chr4:25 995 704–25 995 985) (Supplementary Fig. 1), with weak binding (17 reads) of PSD95-6ZF-NoED at its coding sequence; however, this binding was also found in the IgG sample (Supplementary Fig. 2B).

PSD95-6ZF-fusion constructs induce epigenetic reprogramming and bidirectionally control *Dlg4*/PSD95 gene expression in N2a cells

The 6ZF DNA binding module was fused to various effector domains to induce either activation or repression of the *Dlg4*/PSD95 gene through direct transcriptional or epigenetic mechanisms. To promote robust transcriptional activation of the *Dlg4*/PSD95 gene, we first linked the DNA-binding module of the PSD95-6ZF to the transactivator domain of VP64 (tetramer of viral protein VP16) to generate the ATF PSD95-6ZF-VP64 (Fig. 4A). Conversely, to induce strong transcriptional repression, the PSD95-6ZF module was fused to the SKD to generate ATF PSD95-6ZF-SKD (Fig. 4A). To achieve sustained gene expression modulation, epigenetic editing can be induced by fusing catalytic domains of histone modifying enzymes to a zinc-finger DNA-binding module, generating synthetic ZFPs. Considering that in myoblastic cell-line C2C12 *Dlg4*/PSD95 gene silencing was strongly associated with enrichment of the repressive marks H3K9me2 and H3K9me3 (Fig. 3A and B, black bars), and their histone methyltransferases G9a and SUV39-H1 (Fig. 3C and D, black bars), respectively, we engineered PSD95-6ZF-G9a and PSD95-6ZF-Suvdel76 to induce specific targeted rewriting of histone tails associated with silenced *Dlg4*/PSD95 gene promoters to achieve *Dlg4*/PSD95 gene repression (Fig. 4A).

To investigate whether the PSD95-ZFPs and PSD95-ATFs alter *Dlg4*/PSD95 gene expression through defined epigenetic editing, N2a neuroblastoma cells were infected with retroviruses containing the diverse PSD95-6ZF-fusion constructs and 72 h later *Dlg4*/PSD95 mRNA and PSD95 protein levels were quantified (Fig. 4C and D) and ChIP assays performed (Fig. 4E–H). PSD95-6ZF-G9a and PSD95-6ZF-Suvdel76 produced robust *Dlg4*/PSD95 gene repression (Fig. 4C and D), which was accompanied by strong *de novo* di- and tri-methylation of H3K9, respectively, at the *Dlg4*/PSD95 gene promoter (Fig. 4E and F).

Expression of PSD95-6ZF-SKD also led to *Dlg4*/PSD95 gene repression and a moderate presence of the H3K9me2 and H3K9me3 marks (Fig. 4E and F), indicating that SKD-dependent repression is, in part, mediated by (or resulting in) recruiting histone methyltransferases to the *Dlg4*/PSD95 gene promoter. H3K9me2/3 marks were not observed following infection with GFP (control) or PSD95-6ZF-NoED. ChIP assays furthermore showed that histone H3 proteins levels associated to the *Dlg4*/PSD95 gene promoter were not altered by any of the conditions (Fig. 4G), while expression of PSD95-6ZF fused to SKD, G9a, or Suvdel76 diminished H3 acetylation (Fig. 4H).

Conversely, we demonstrated that expression of PSD95-6ZF-VP64 strongly enhanced levels of *Dlg4*/PSD95 mRNA (Fig. 4C). At the protein level, PSD95-6ZF-VP64 increased PSD95 expression only slightly in N2a cells (Fig. 4D, upper blots) but more robustly in hippocampal neurons (Fig. 4D, lower blots). Further analyses of N2a cells revealed that enhanced *Dlg4*/PSD95 gene expression was accompanied by a strong increase in the presence of the H3ac mark (Fig. 4H), suggesting that PSD95-6ZF-VP64 contributes to transcriptional activation of the *Dlg4*/PSD95 gene through (direct or indirect) recruitment of histone acetyltransferases.

Using bisulfite sequencing analysis, we found that none of the 12 CpGs sites located in the *Dlg4*/PSD95 proximal gene promoter sequence were methylated following transduction with any of the PSD95-6ZF-fusion constructs (Fig. 4I). Collectively, our results indicate that PSD95-6ZF-G9a, PSD95-6ZF-Suvdel76, and PSD95-6ZF-SKD repress *Dlg4*/PSD95 gene expression by epigenetic reprogramming of histone H3 associated with the *Dlg4*/PSD95 gene promoter, without methylating the promoter DNA sequence. Conversely, the designed ATF PSD95-6ZF-VP64 activates *Dlg4*/PSD95 gene expression by increasing activating histone post-translational modification.

Phenotypic rescue experiments were conducted in hippocampal cultures to demonstrate the specificity of the PSD95-6ZF-fusion constructs and to rule out off-target effects. Given that large scale dendritic structural alterations of cultured hippocampal neurons are highly influenced by *Dlg4*/PSD95 gene expression (Charych *et al.*, 2006; Henriquez *et al.*, 2013; Bustos *et al.*, 2014), the effects of the PSD95-6ZF-fusion constructs on hippocampal dendritogenesis in the absence and presence of conventional gain (cDNA) and loss (RNAi) of function approaches were determined. We found that expression of short-hairpin RNA that knocked-down *Dlg4*/PSD95 counteracted PSD95-6ZF-VP64-mediated reduction of dendritogenesis (Supplementary Fig. 3A and B). Conversely, overexpression

of *Dlg4*/PSD95 cDNA neutralized the effects of PSD95-6ZF-SKD (Supplementary Fig. 3C and D).

PSD95-6ZF-fusion constructs are effective modulators of *Dlg4*/PSD95 gene expression *in vivo* and affect plasticity-associated processes

Previous gain- and loss-of-function studies revealed a critical role for PSD95 in dendritic spine maturation, as visualized by the ratio of mature mushroom spines versus filopodia-like structures (El-Husseini *et al.*, 2000; Ehrlich *et al.*, 2007; Bustos *et al.*, 2014). We wanted to determine if modulation of *Dlg4*/PSD95 expression levels with our novel PSD95-6ZF-fusion constructs was an effective approach to control spine morphology *in vivo*. To achieve this, we used recombinant HSV vectors with the PSD95-6ZF-fusion cDNAs placed under the IE4/5 promoter and enhanced green fluorescent protein (eGFP) expression driven by a CMV promoter to visualize transduced cells (Fig. 5A). HSV vectors expressing only eGFP under the CMV promoter were used as control (HSV-Ctrl). HSV-mediated transgene expression is fast (within hours) and robust, facilitating detailed morphological analyses. Because HSV-mediated transgene expression peaks at Day 3 and then largely dissipates by Day 6 (Barrot *et al.*, 2002; data not shown), all the experiments with this virus were performed at 3–4 days post-infection (dpi).

We found that infection of hippocampal cells *in vivo* with HSV-PSD95-6ZF-Suvdel76 or HSV-PSD95-6ZF-VP64 led to decreased or increased *Dlg4*/PSD95 mRNA expression, respectively, relative to HSV-Ctrl (Fig. 5B). Next, we examined if expression of the specific PSD95-6ZF-fusion constructs regulates spine maturation. To accomplish this, we infected the dentate gyrus of the hippocampus in 8-month-old mice with the specific HSVs and analysed spine morphology and density 3 dpi (Fig. 5C–G). Dendritic protrusions on second order branches of selected granular cells were classified based on their size and shape. As shown earlier (Jain *et al.*, 2012; Ampuero *et al.*, 2017), granular cells in mature mice display substantial numbers of thin, stubby and mushroom spines, and had few filopodia (Fig. 5D–G). Overall spine density was maintained in neurons expressing PSD95-6ZF-Suvdel76 or PSD95-6ZF-VP64 (Fig. 5E). Consistent with findings that PSD95 participates in spine maturation *in vitro* (El-Husseini *et al.*, 2000; Ehrlich *et al.*, 2007; Bustos *et al.*, 2014), dentate gyrus neurons expressing PSD95-6ZF-VP64 led to a higher density of mushroom spines (Fig. 5F), that displayed an increased volume (Fig. 5G). Expression of PSD95-6ZF-Suvdel76 *in vivo* for 3 days did not affect these parameters (Fig. 5F and G).

In vitro and *in vivo* studies also have documented that PSD95 impacts the maturation of synapses by regulating the synaptic expression of AMPA receptors (El-Husseini *et al.*, 2000; Ehrlich *et al.*, 2007; Elias *et al.*, 2008) and of NMDA receptors (Losi *et al.*, 2003; van Zundert *et al.*, 2004; Elias *et al.*, 2008; Bustos *et al.*, 2014). To determine whether our PSD95-6ZF-fusion constructs alter excitatory synaptic transmission, dentate gyrus neurons in adult mice were infected with the specific HSVs, and 3–4 dpi acute slices were prepared to perform electrophysiological recordings from GFP-positive neurons. Our data indicate that HSV-PSD95-6ZF-Suvdel76 yielded a significant decrease in the NMDA/AMPA ratio relative to control, that seemed to be the result of a strong decrease in NMDA-mediated eEPSCs and, to a lesser extent, in AMPA-mediated eEPSCs (Fig. 5H and I). The NMDA/AMPA ratio in neurons infected with HSV-PSD95-6ZF-VP64 was similar to controls, and appeared to be the result of increases in both eEPSC NMDA receptors and eEPSC AMPA receptors (Fig. 5H and I). Paired pulse ratios were not significantly different between HSV-Ctrl ($91 \pm 8\%$; $n = 6$), HSV-PSD95-6ZF-Suvdel76 ($97 \pm 8\%$; $n = 5$), and HSV-PSD95-6ZF-VP64 ($110 \pm 8\%$; $n = 5$), indicating that presynaptic release of glutamate was similar in the different conditions. Together, our studies in mice demonstrate that modulation of *Dlg4*/PSD95 gene expression by engineered PSD95-6ZF-fusion constructs targeting the *Dlg4*/PSD95 locus is sufficient to regulate synapse and spine maturation of hippocampal neurons *in vivo*.

PSD95-6ZF-VP64 improves learning and memory deficits in aged and AβPPswe/PS-1 mice

We also examined if PSD95-6ZF-VP64 transduction could recover learning and memory deficits in aged mice and in a mouse model of Alzheime's disease (AβPPswe/PS-1); both models display memory impairments accompanied by a loss of PSD95 expression (de Bartolomeis *et al.*, 2014; Savioz *et al.*, 2014; Hong *et al.*, 2016). We used a novel object recognition (NOR) test, a simple single trial behavioural memory task that relies primarily on a rodent's innate preference for novel versus familiar objects when allowed to explore freely; specifically, hippocampal-mediated memory impairments are evidenced when animals do not discriminate between a novel and familiar object 24 h after training. As expected, aged wild-type mice (15–18-month-old) performed poorly in the NOR test, showing limited exploration of the novel objects relative to younger (5-month-old) wild-type mice (Supplementary Fig. 4). Next, aged animals were equally divided in two groups and bilaterally injected in the hippocampus (CA1 and dentate gyrus) with either HSV-Ctrl or HSV-PSD95-6ZF-VP64, and animals were tested for NOR 3 dpi. Interestingly, our results revealed that treatment with HSV-PSD95-6ZF-VP64, but not HSV-Ctrl, reverted the NOR impairment in aged mice, reaching levels comparable to those found in young mice (Supplementary Fig. 4).

Next, we evaluated if PSD95-6ZF-VP64 transduction could prevent or recover hippocampal dysfunction associated with learning and memory deficits in AβPPswe/PS-1

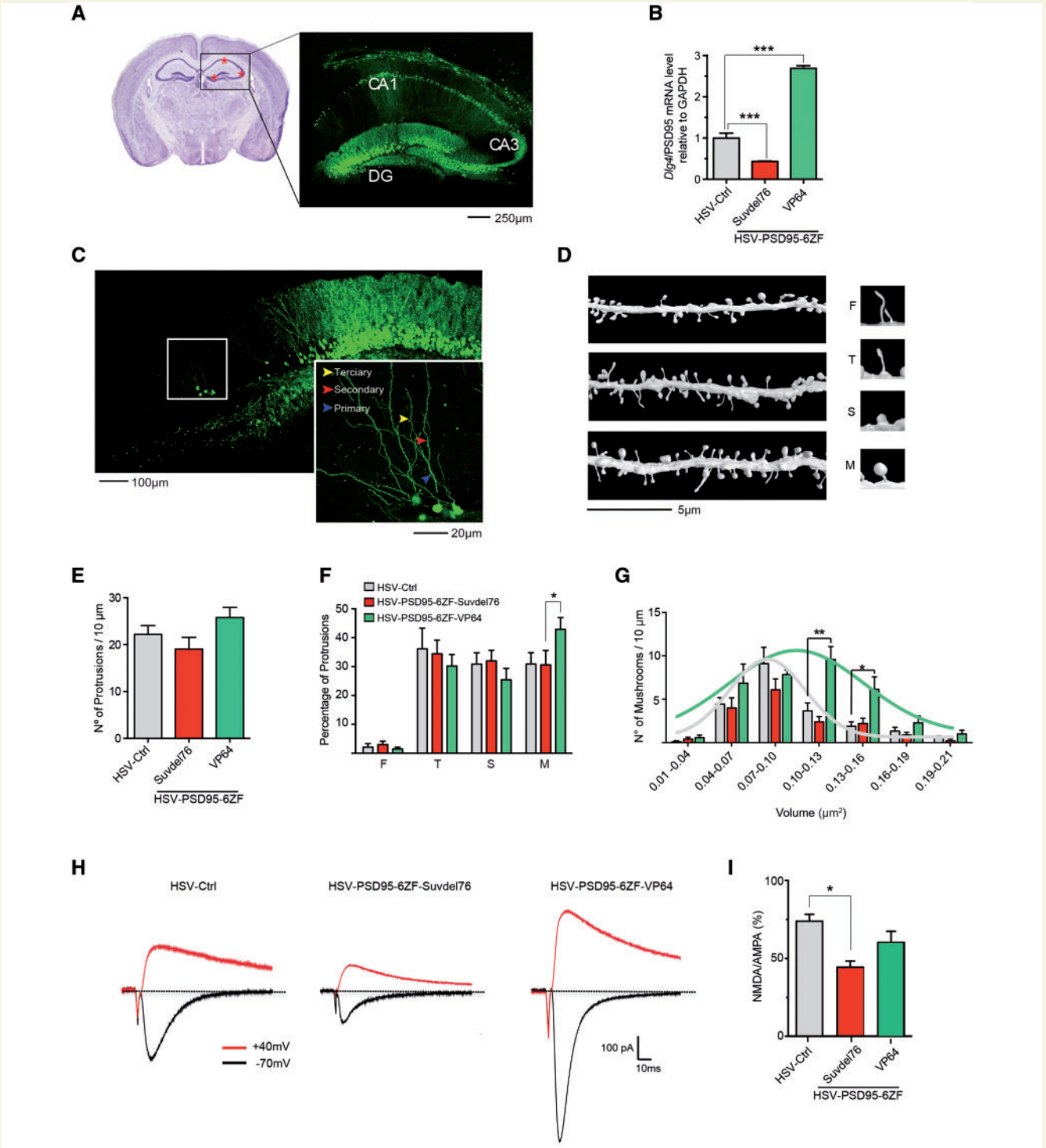

Figure 5 Viral-mediated expression of PSD95-6ZF-fusions in the hippocampus *in vivo* regulate spine morphology and AMPA receptor-mediated synaptic activity. HSV vectors expressing eGFP alone (HSV-Ctrl), eGFP plus PSD95-6ZF-Suvdel76 (HSV-PSD95-6ZF-Suvdel76), or eGFP plus PSD95-6ZF-VP64 (HSV-PSD95-6ZF-VP64) were generated. (**A**) Mice were injected bilaterally with HSVs into the CA1, CA3 and dentate gyrus (DG) (indicated by the asterisk). Three days post-injection (dpi), hippocampi were isolated, fixed, and sliced to show infection efficiency by confocal microscopy. (**B**) To measure *Dlg4*/PSD95 mRNA levels by qRT-PCR, dorsal hippocampi were isolated 6 hr post-injection. (**C–I**) For spine morphology and electrophysiology, 8-week-old mice were only injected into dentate gyrus; 3 dpi, slices were prepared on (**C–G**) fixed or (**H** and **I**) unfixed brain. (**C**) Fluorescent images at 10× or 60× (*inset*) show infected dentate gyrus neurons; only secondary dendritic processes were analysed. (**D**) 3D active surface models of dendrite morphology. Dendritic protrusions or spines were classified as filopodia (F), thin (T), stubby (S), or mushroom (M). (**E–G**) Graphs show quantification of (**E**) spine density, (**F**) spine morphology, or (**G**) mushroom volume of dentate gyrus neurons expressing the diverse PSD95-6ZF constructs. (**H**) Using whole-cell patch-clamp recordings, eEPSCs of GFP-positive dentate gyrus neurons were analysed. Representative traces of neurons infected with HSV-Ctrl, HSV-PSD95-6ZF-Suvdel76, or HSV-PSD95-6ZF-VP64 are shown. (**I**) Quantification of average NMDA/AMPA ratios as indicated. Bars represent means ± SEM from five to six neurons per condition; statistical analysis was performed using Student's *t*-test. $*P < 0.05$, $**P < 0.01$, $***P < 0.001$, relative to control.

mice. As expected, all non-infected AβPPswe/PS-1 mice (6 months old) performed poorly in the NOR test, compared to age-matched wild-type mice (Fig. 6A–D). Next, AβPPswe/PS-1 mice were equally divided in two groups and injected bilaterally in the hippocampus with either recombinant AAV vectors encoding PSD95-6ZF-VP64 plus GFP (AAV-PSD95-6ZF-VP64) or only GFP as control (AAV-Ctrl) (scheme in Fig. 6A). Given that AAVs allow long-term transgene expression *in vivo* with limited (or undetected) toxicity, AAVs are the preferential vehicles for gene therapy, including for patients suffering brain diseases (Mingozzi and High, 2013). To achieve stable and widespread transgene expression in the hippocampus, AAV vectors with the novel PHP.B capsid were generated (Deverman *et al.*, 2016). We found that AβPPswe/PS-1 mice (6–8 months old) infected for 2.5 weeks with AAV-PSD95-6ZF-VP64 expressed significant increased PSD95 protein levels relative to animals injected with AAV-Ctrl [1.26 ± 0.08 ($n = 4$ per condition); $^{*}P < 0.05$ Student's *t*-test; Fig. 6B]. Importantly, treatment of AβPPswe/PS-1 mice (6.5 months old) for 2.5 weeks with AAV-PSD95-6ZF-VP64, but not AAV-Ctrl, rescued the NOR impairment, reaching levels comparable to wild-type mice (Fig. 6C and D). Additionally, these AAV-PSD95-6ZF-VP64-treated AβPPswe/PS-1 mice improved in the object location memory (OLM) test, a simple single trial spatial memory task (Supplementary Fig. 5). Subsequently, we tested the same AβPPswe/PS-1 mice for spatial learning performance using an adapted Morris water maze task. The Morris water maze task relies on distal cues that guide rodents from start locations around the perimeter of an open circular water maze to locate a submerged escape platform. Memory flexibility, in which the platform is changed each day, has been proven more sensitive than the classical Morris water maze task to evaluate hippocampal-dependent spatial-based learning and memory across several days (Chen *et al.*, 2000; Serrano *et al.*, 2014). Memory flexibility was not affected in AβPPswe/PS-1 mice until they reached 12 months of age (data not shown). Interestingly, and as indicated by the fewer trials to achieve the learning criterion, we found that AAV-PSD95-6ZF-VP64-treated AβPPswe/PS-1 mice showed significantly improved memory flexibility scores relative to untreated and AAV-GFP-treated AβPPswe/PS-1 animals, reaching levels that are comparable to those found in young 5-month-old wild-type mice (Fig. 6E).

After testing memory flexibility, mice were sacrificed to determine infection efficiency and PSD95 expression levels. Confocal images show robust GFP expression in the soma and projections of hippocampal pyramidal neurons of AβPPswe/PS-1 mice infected with AAV-PSD95-6ZF-VP64 or AAV-Ctrl (Fig. 6F). Finally, we determined whether AAV-PSD95-6ZF-VP64 increased PSD95 protein expression at hippocampal synapses in AβPPswe/PS-1 mice. To achieve this, synaptic membranes of pooled hippocampi (three mice/condition) were prepared. We found increased synaptic PSD95 protein levels in AβPPswe/PS-1 mice (12 months old) infected 5 months earlier with AAV-PSD95-6ZF-VP64 relative to animals injected with AAV-Ctrl (Fig. 6G, upper blots). Homogenates of these same pooled samples revealed that total PSD95 protein levels were also increased in AβPPswe/PS-1 mice treated with AAV-PSD95-6ZF-VP64 (Fig. 6G, lower blots). To determine total PSD95 protein levels of individual hippocampi, in independent experiments AβPPswe/PS-1 mice (7 months old) were treated for 5 months with AAV-PSD95-6ZF-VP64 or AAV-PSD95-6ZF-NoED, as control. Expression of PSD95-6ZF constructs containing VP64, but no effector domain (NoED), increased PSD95 protein levels in individual hippocampi derived from 12-month-old AβPPswe/PS-1 mice, reaching levels comparable to those found in age-matched wild-type mice (Supplementary Fig. 6). Together, we found that transduction of the ATF PSD95-VP64 increased PSD95 expression and rescued memory deficits in aged and Alzheimer's disease mice.

Discussion

Here we elucidated epigenetic mechanisms that control *Dlg4*/PSD95 gene expression during rat hippocampus development. The established epigenome landscape, together with the generation of PSD95-6ZF-fusion constructs, allowed us to alter the expression of *Dlg4*/PSD95 through epigenetic mechanisms. The PSD95-6ZF-fusion constructs regulated various neural plasticity-associated processes and validated PSD95 as a key player in plasticity and memory. Importantly, this work also establishes epigenome editing as a potential therapy to treat human neurological disorders with PSD95-dependent cognitive impairments. Use of zinc finger constructs to alter gene expression has advantages over more conventional loss- and gain-of-function approaches. First, engineered transcription factors can regulate expression of mRNAs that include all potential splice variants in a physiological context. This could be important for PSD95 as it has been demonstrated that expression of PSD95 isoforms is required to mediate synaptic strengthening by activity-dependent and activity-independent mechanisms (Schlüter *et al.*, 2006). Second, engineered transcription factors have been shown to induce long-lasting changes in gene expression when fused to effector domains that alter histone tail modifications or the methylation status of genomic DNA sequences (de Groote *et al.*, 2012; Stolzenburg *et al.*, 2015). Importantly, although studies in cell lines indicate that the maintenance of induced epigenetic modifications is dependent on the genomic context of the cells (Kungulovski *et al.*, 2015; Cano-Rodriguez *et al.*, 2016), stability of epigenetic alterations by epigenome editing tools has not been assessed in post-mitotic cells such as neurons.

Repressive histone post-translational modifications and DNA methylation contribute to prevent the expression of certain genes and enable cells to define a specific identity (Bannister and Kouzarides, 2011; Gardner *et al.*, 2011). Surprisingly, however, the proximal *Dlg4*/PSD95 gene promoter in hippocampal cells lacks the classic repressive histone marks H3K27me3 (Henriquez *et al.*, 2013) and

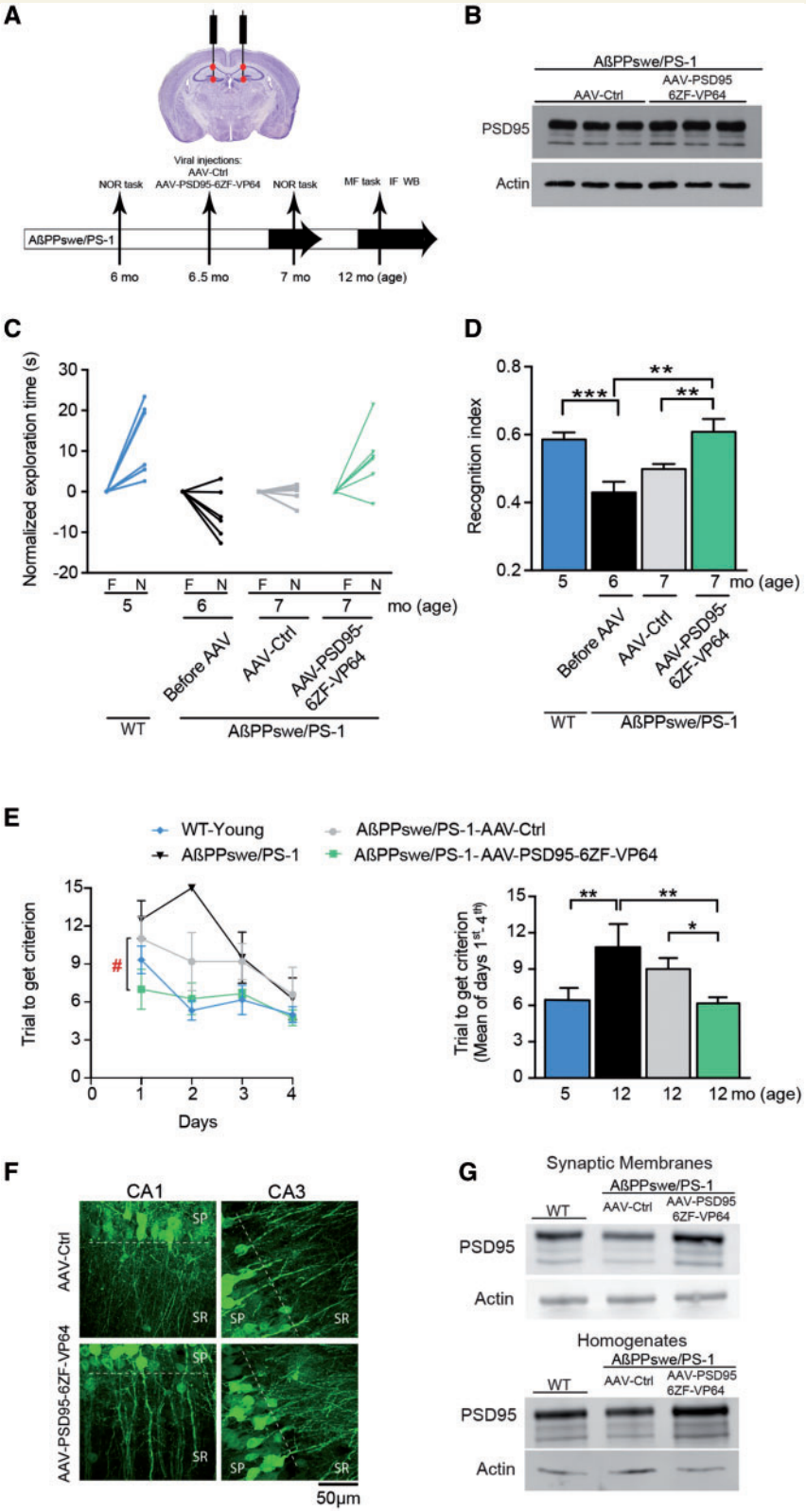

Figure 6 AAV-PSD95-6ZF-VP64 treatment improves NOR and memory flexibility performances in AβPPswe/PS-1 mice. (**A**) Scheme of experiment. AAV-PHP.B carrying GFP alone (AAV-Ctrl) or GFP plus PSD95-6ZF-VP64 (AAV-PSD95-6ZF-VP64) were generated and injected in 6.5-month-old AβPPswe/PS-1 mice into the hippocampus (CA1 and dentate gyrus, as indicated by red dots). NOR task was performed before (age 6 months) and after (age 7 months) AAV injections. After testing memory flexibility (MF) (age 12 months), mice were sacrificed to test infection efficiency by immunofluorescence (IF) and PSD95 expression levels by western blot (WB), respectively. (**B**) Total PSD95 protein levels were analysed by western blot using total protein extracts from individual hippocampi derived from AβPPswe/PS-1 mice

(continued)

H3K9me2/3 (tested here), nor does it show DNA methylation, even during embryonic development when *Dlg4*/PSD95 expression is limited. Consistent with our findings, public epigenomic databases with genome-wide mapping (ENCODE Project Consortium, 2012; Roadmap Epigenomics Consortium *et al.*, 2015) reveal a lack of H3K27me3 marking and DNA methylation, and show a light (though extensively distributed) marking of H3K9me3 at the proximal *Dlg4*/PSD95 promoter in mouse and human brain tissue, including in the foetal hippocampus. A similar absence of well-defined repressive epigenetic marking is observed at the *Dlg4*/PSD95 promoter in mouse and human embryonic stem cells, where this gene is not transcribed. In contrast to the *Dlg4*/PSD95 gene promoter, the epigenetic signature of proximal promoters of other synaptic plasticity genes (i.e. those encoding AMPA receptors, NMDA receptors and CaMKII) is not consistent among the diverse epigenomic databases. For example, the promoter region of *GRIA1*/GluR1 subunit of the AMPA receptor is marked $H3K9me3^{+}/H3K27me3^{+}$ in human embryonic stem cells, $H3K9me3^{-}/H3K27me3^{+}$ in human foetal female whole brain (17 weeks), $H3K9me3^{-}/H3K27me3^{-}$ in mouse embryonic stem cells, and $H3K9me3^{+}/H3K27me3^{-}$ in mouse embryonic whole brain (embryonic Day 14.5) (ENCODE Project Consortium, 2012; Roadmap Epigenomics Consortium *et al.*, 2015). Why such discrepancies occur is unclear, but they highlight the need for validating histone post-translational modification patterns in specific loci of the biological material of interest before performing epigenomic editing to test causal links to given traits or diseases.

In addition to repressive marks, here we show that typical activating marks (i.e. H3K9ac, H3K27ac, H3K4me3) are minimally present at the *Dlg4*/PSD95 gene promoter in embryonic hippocampal cells, similarly as shown in embryonic stem cells (ENCODE Project Consortium, 2012; Roadmap Epigenomics Consortium *et al.*, 2015). As the hippocampus develops, however, these activating marks are increasingly deposited at the *Dlg4*/PSD95 gene promoter. Concurrently, we found an increased enrichment of CBP/p300, GCN5, and Wdr5 at the *Dlg4*/PSD95 gene promoter, chromatin-modifying enzymes and complexes implicated in depositing H3K9ac, H3K27ac and H3K4me3, respectively (Bannister and Kouzarides, 2011). These enzymes are also implicated in recruiting RNA polymerase cofactors (Bannister and Kouzarides, 2011), and in agreement, we previously found that active RNA polymerase II is enriched at the *Dlg4*/PSD95 gene promote during hippocampal development (Henriquez *et al.*, 2013). We also detected that phosphorylated CREB is increasingly enrichment at the *Dlg4*/PSD95 gene promoter during hippocampal development (not shown). Calcium influx through stimulated synaptic NMDA receptors, or voltage-sensitive calcium channels, results in phosphorylation and hence activation of CREB to initiate a transcriptional program of plasticity-associated genes (including *Dlg4*/PSD95) that drives spine maturation (West *et al.*, 2001; West and Greenberg, 2011). Given that phosphorylated CREB (Hardingham *et al.*, 1999) and GCN5 (Agalioti *et al.*, 2000) recruit CBP to promoters, alone or with the highly homologous co-activator p300, the presented work also provides important insights in how signalling pathways regulate epigenetic processes to control *Dlg4*/PSD95 gene expression during rat hippocampus development.

To demonstrate a causal relationship between epigenetic modifications at the plasticity *Dlg4*/PSD95 gene promoter and its expression, we engineered PSD95-6ZF-fusion constructs. The proximal *Dlg4*/PSD95 promoter region (−38 to −21) was selected because it is: (i) close to the transcription start sites of the *Dlg4*/PSD95 gene promoter, a region that typically is poorly enriched in nucleosomes (Jiang and Pugh, 2009), enabling greater access to transcription factors, including ZFPs; and (ii) highly conserved

Figure 6 Continued
treated for 2.5 weeks with AAV-Ctrl or AAV-PSD95-6ZF-VP64 at 6–8 months old. Actin was used as loading control. (**C** and **D**) Single-trail NOR was performed on AβPPswe/PS-1 mice and wild-type mice and shown as (**C**) normalized exploration time and (**D**) recognition index. The recognition index corresponds to the time spent to explore the novel object, divided by the total time spent exploring both objects; an index of 0.5 indicates that mice do not discriminate between a novel and familiar object. Values represent mean ± SEM from ⩾6 mice per condition. Statistical analysis was performed using one-way ANOVA followed by Bonferroni *post hoc* test. $^{**}P < 0.01$, $^{***}P < 0.001$. See also Supplementary Fig. 5 for additional OLM test performed after NOR. (**E**) The continuous multiple-trial memory flexibility task was performed for 4 days on 12-month-old AβPPswe/PS-1 mice and 5-month-old young wild-type mice 24 h after training. Values represent mean ± SEM from ⩾4–6 mice per condition for both (*left*) line and (*right*) bar graph. Two-way ANOVA followed by Bonferroni *post hoc* test for the line graph (*left*) revealed significant differences in the learning curve (Days 1–4): $^{\#}P < 0.05$ AAV-PSD95-6ZF-VP64-treated AβPPswe/PS-1 mice relative to AAV-GFP-treated AβPPswe/PS-1 mice (hash symbol shown in red in *left* panel); $^{\#\#\#}P < 0.001$ (not shown) untreated AβPPswe/PS-1 mice relative to AAV-PSD95-6ZF-VP64-treated AβPPswe/PS-1 mice and young wild-type. For simplicity, bar plot (*right*) shows the average mean of trail to criterion for Days 1 to 4. One-way ANOVA followed by Bonferroni *post hoc* test revealed significant differences as indicated: $^{*}P < 0.05$ and $^{**}P < 0.01$. (**F**) Representative confocal image of CA1 and CA3 12-month-old AβPPswe/PS-1 mice infected with (*top row*) AAV-Ctrl or (*bottom row*) AAV-PSD95-6ZF-VP64 at age 6.5 months. High GFP levels are observed in pyramidal neurons with their soma located in the stratum pyramidale (SP) and their dendrites projecting into the stratum radiatum (SR). (**G**) Western blot of synaptic membranes (*top* blots) and homogenates (*bottom* blots) of pooled hippocampi from three mice per condition: Control 12–15-month-old wild-type mice (WT), 12-month-old AβPPswe/PS-1 mice treated with AAV-Ctrl or AAV-PSD95-6ZF-VP64 at age 6.5 months. Expression of PSD95 and actin (loading control) are shown.

across diverse vertebrate species, sharing 100% identity across mouse, rat and human. We found that PSD95-6ZF fused to G9a, Suvdel76, or SKD repressed *Dlg4*/PSD95 expression concomitant with *de novo* di- and tri-methylation of H3K9 at the *Dlg4*/PSD95 gene promoter. In non-neuronal cells, it has been documented that the H3K9me2/3 mark maintains and spreads heterochromatin by creating a docking site for chromodomain-containing proteins, like heterochromatin protein 1 (HP1), which in turn recruits DNA methyltransferases and/or nucleosome remodellers (Smith and Meissner, 2013). However, *de novo* H3K9 methylation at the *Dlg4*/PSD95 gene promoter in N2a cells is neither associated with CpG methylation nor with increased enrichment of histone H3, arguing against heterochromatin formation at the *Dlg4*/PSD95 gene locus by the engineered ZFPs in our experimental set-up. We also found that H3K9 methylation is correlated with a reduced acetylation of histone H3 in N2a cells that express PSD95-6ZF fused to G9a, Suvdel76, or SKD. Similar G9a-containing ZFPs induce hypo-acetylation in some cell types (cancer cell lines; Falahi *et al.*, 2013), but not in others (neurons; Heller *et al.*, 2014). Whether the H3K9me2/3 mark recruits epigenetic enzymes that alter the DNA methylation, and/or the histone acetylation status, thus likely depends on the gene- and/or chromatin context of the target cell. We also found that the designed ATF PSD95-6ZF-VP64 activates *Dlg4*/PSD95 gene expression, at least in part through epigenetic mechanisms involving increased H3 acetylation.

We further demonstrated that the engineered PSD95-6ZF-fusion constructs altered PSD95 levels, synapse and spine maturation in hippocampal neurons *in vivo*. More importantly, we also show that the PSD95-ATF rescues recognition memory deficits in aged mice and a mouse model of Alzheimer's disease. This is the first study that establishes gene targeting as a potential therapy to ameliorate memory impairments in human neurological disorders.

In conclusion, our study has broad biological implications as the hippocampal epigenome analysis and targeted epigenetic editing with the novel designed PSD95-6ZF-fusion constructs provide important insights into the epigenetic mechanisms underlying neuronal plasticity and learning and memory. Our work also has broad therapeutic implications as the novel designed engineered transcription factors specifically and efficiently bind to the rat *Dlg4*/PSD95 locus in hippocampal neurons at a target sequence that is highly conserved across vertebrate species (100% identity among mice, rats, and humans). Thus, our novel engineered PSD95-6ZF-fusion constructs are attractive candidates for future gene therapies in several human central and peripheral nervous system disorders where *Dlg4*/PSD95 expression is reduced (e.g. ageing, Alzheimer's disease, Huntington's disease) or increased (e.g. pain disorders) (Arbuckle *et al.*, 2010; Savioz *et al.*, 2014; Zhang *et al.*, 2014; Hong *et al.*, 2016).

Acknowledgements

We thank Fabiola Rojas and Luis Melo for their technical support and BioPub for revising the manuscript.

Funding

This work was supported by Fondecyt 1140301, ALS Therapy Alliance-2014-F-034, Anillo-RING ACT1114, and FONDEQUIP EQM 140166 (B.v.Z.); DRI USA 2013-0030 (B.v.Z., L.V.-N., M.M.); Nucleus DI-603-14/N and DI-4-17/N (B.v.Z., L.V.-N., J.S.); FONDAP 15090007 and Fondecyt 1170878 (M.M.); FP7-PEOPLE-2011-IRSES EULAMDIMA (B.v.Z., M.M.); Conicyt 24110099 (F.J.B.), Fondecyt-3130582 (E.A.); Conicyt 201161486 (N.J.); Fondecyt 1150933 (L.V.-N.); Fondecyt 3110138 (B.H.); FONDECYT 1130614, Anillo ACT-1414 and Millennium Nucleus NUMIND (NC-130011) Millenium Scientific Initiative of the Ministry of Economy, Development and Tourism (Chile) (M.F.); Fondecyt 1151029, FONDEQUIP EQM140119, CONICYT PIA ACT1402, ICM P09-015-F, CORFO 16CTTS-66390 and DAAD 57220037 & 57168868 CONICYT-PFB 12/2007 (J.T., S.H.). Basal Center of Excellence in Aging and Regeneration (N.C.I.). NIH/NINDS grant NS093941 (M.S-E).

Supplementary material

Supplementary material is available at *Brain* online.

References

Agalioti T, Lomvardas S, Parekh B, Yie J, Maniatis T, Thanos D. Ordered recruitment of chromatin modifying and general transcription factors to the IFN-beta promoter. Cell 2000; 103: 667–78.

Ampuero E, Jury N, Härtel S, Marzolo M-P, van Zundert B. Interfering of the Reelin/ApoER2/PSD95 signaling axis reactivates dendritogenesis of mature hippocampal neurons. J Cell Physiol 2017; 232: 1187–99.

Arbuckle MI, Komiyama NH, Delaney A, Coba M, Garry EM, Rosie R, et al. The SH3 domain of postsynaptic density 95 mediates inflammatory pain through phosphatidylinositol-3-kinase recruitment. EMBO Rep 2010; 11: 473–8.

Bannister AJ, Kouzarides T. Regulation of chromatin by histone modifications. Cell Res 2011; 21: 381–95.

Barrot M, Olivier JDA, Perrotti LI, DiLeone RJ, Berton O, Eisch AJ, et al. CREB activity in the nucleus accumbens shell controls gating of behavioral responses to emotional stimuli. Proc Natl Acad Sci USA 2002; 99: 11435–40.

Beltran AS, Blancafort P. Reactivation of MASPIN in non-small cell lung carcinoma (NSCLC) cells by artificial transcription factors (ATFs). Epigenetics 2011; 6: 224–35.

Broekman MLD, Comer LA, Hyman BT, Sena-Esteves M. Adeno-associated virus vectors serotyped with AAV8 capsid are more efficient than AAV-1 or -2 serotypes for widespread gene delivery to the neonatal mouse brain. Neuroscience 2006; 138: 501–10.

Bustos FJ, Jury N, Martinez P, Ampuero E, Campos M, Abarzúa S, et al. NMDA receptor subunit composition controls dendritogenesis

of hippocampal neurons through CAMKII, CREB-P, and H3K27ac. J Cell Physiol 2017; 27: 8334.
Bustos FJ, Varela-Nallar L, Campos M, Henriquez B, Phillips M, Opazo C, et al. PSD95 suppresses dendritic arbor development in mature hippocampal neurons by occluding the clustering of NR2B-NMDA receptors. PLoS One 2014; 9: e94037.
Cano-Rodriguez D, Gjaltema RAF, Jilderda LJ, Jellema P, Dokter-Fokkens J, Ruiters MHJ, et al. Writing of H3K4Me3 overcomes epigenetic silencing in a sustained but context-dependent manner. Nat Commun 2016; 7: 12284.
Cedar H, Bergman Y. Programming of DNA methylation patterns. Annu Rev Biochem 2012; 81: 97–117.
Charych EI, Akum BF, Goldberg JS, Jörnsten RJ, Rongo C, Zheng JQ, et al. Activity-independent regulation of dendrite patterning by post-synaptic density protein PSD-95. J Neurosci 2006; 26: 10164–76.
Chen G, Chen KS, Knox J, Inglis J, Bernard A, Martin SJ, et al. A learning deficit related to age and beta-amyloid plaques in a mouse model of Alzheimer's disease. Nature 2000; 408: 975–9.
Chen H, Kazemier HG, de Groote ML, Ruiters MHJ, Xu GL, Rots MG. Induced DNA demethylation by targeting Ten-Eleven Translocation 2 to the human ICAM-1 promoter. Nucleic Acids Res 2014; 42: 1563–74.
de Bartolomeis A, Latte G, Tomasetti C, Iasevoli F. Glutamatergic postsynaptic density protein dysfunctions in synaptic plasticity and dendritic spines morphology: relevance to schizophrenia and other behavioral disorders pathophysiology, and implications for novel therapeutic approaches. Mol Neurobiol 2014; 49: 484–511.
de Groote ML, Verschure PJ, Rots MG. Epigenetic Editing: targeted rewriting of epigenetic marks to modulate expression of selected target genes. Nucleic Acids Res 2012; 40: 10596–613.
Dekker AD, De Deyn PP, Rots MG. Epigenetics: the neglected key to minimize learning and memory deficits in down syndrome. Neurosci Biobehav Rev 2014; 45: 72–84.
Deverman BE, Pravdo PL, Simpson BP, Kumar SR, Chan KY, Banerjee A, et al. Cre-dependent selection yields AAV variants for widespread gene transfer to the adult brain. Nat Biotechnol 2016; 34: 204–9.
Ehrlich I, Klein M, Rumpel S, Malinow R. PSD-95 is required for activity-driven synapse stabilization. Proc Natl Acad Sci USA 2007; 104: 4176–81.
El-Husseini AE, Craven SE, Chetkovich DM, Firestein BL, Schnell E, Aoki C, et al. Dual palmitoylation of PSD-95 mediates its vesiculotubular sorting, postsynaptic targeting, and ion channel clustering. J Cell Biol 2000; 148: 159–72.
Elias GM, Elias LAB, Apostolides PF, Kriegstein AR, Nicoll RA. Differential trafficking of AMPA and NMDA receptors by SAP102 and PSD-95 underlies synapse development. Proc Natl Acad Sci USA 2008; 105: 20953–8.
Elias GM, Nicoll RA. Synaptic trafficking of glutamate receptors by MAGUK scaffolding proteins. Trends Cell Biol 2007; 17: 343–52.
ENCODE Project Consortium. An integrated encyclopedia of DNA elements in the human genome. Nature 2012; 489: 57–74.
Falahi F, Huisman C, Kazemier HG, van der Vlies P, Kok K, Hospers GAP, et al. Towards sustained silencing of HER2/neu in cancer by epigenetic editing. Mol Cancer Res 2013; 11: 1029–39.
Falahi F, Sgro A, Blancafort P. Epigenome engineering in cancer: fairy-tale or a realistic path to the clinic? Front Oncol 2015; 5: 22.
Frost B, Hemberg M, Lewis J, Feany MB. Tau promotes neurodegeneration through global chromatin relaxation. Nat Neurosci 2014; 17: 357–66.
Fuenzalida M, Fernandez de Sevilla D, Buno W. Changes of the EPSP waveform regulate the temporal window for spike-timing-dependent plasticity. J Neurosci 2007; 27: 11940–8.
Gaj T, Gersbach CA, Barbas CF III. ZFN, TALEN, and CRISPR/Cas-based methods for genome engineering. Trends Biotechnol 2013; 31: 397–405.
Gardner KE, Allis CD, Strahl BD. Operating on chromatin, a colorful language where context matters. J Mol Biol 2011; 409: 36–46.
Gräff J, Kim D, Dobbin MM, Tsai LH. Epigenetic regulation of gene expression in physiological and pathological brain processes. Physiol Rev 2011; 91: 603–49.
Gräff J, Rei D, Guan J-S, Wang W-Y, Seo J, Hennig KM, et al. An epigenetic blockade of cognitive functions in the neurodegenerating brain. Nature 2013; 483: 222–6.
Hardingham GE, Chawla S, Cruzalegui FH, Bading H. Control of recruitment and transcription-activating function of CBP determines gene regulation by NMDA receptors and L-type calcium channels. Neuron 1999; 22: 789–98.
Härtel K, Singaravelu K, Kaiser M, Neusch C, Hülsmann S, Deitmer JW. Calcium influx mediated by the inwardly rectifying K + channel Kir4.1 (KCNJ10) at low external K + concentration. Cell Calcium 2007; 42: 271–80.
Heller EA, Cates HM, Peña CJ, Sun H, Shao N, Feng J, et al. Locus-specific epigenetic remodeling controls addiction- and depression-related behaviors. Nat Neurosci 2014; 17: 1720–7.
Heller EA, Hamilton PJ, Burek DD, Lombroso SI, Peña CJ, Neve RL, et al. Targeted epigenetic remodeling of the Cdk5 gene in nucleus accumbens regulates cocaine- and stress-evoked behavior. J Neurosci 2016; 36: 4690–7.
Henriquez B, Bustos FJ, Aguilar R, Becerra A, Simon F, Montecino M, et al. Ezh1 and Ezh2 differentially regulate PSD-95 gene transcription in developing hippocampal neurons. Mol Cell Neurosci 2013; 57: 130–43.
Hilton IB, D'Ippolito AM, Vockley CM, Thakore PI, Crawford GE, Reddy TE, et al. Epigenome editing by a CRISPR-Cas9-based acetyltransferase activates genes from promoters and enhancers. Nat Biotechnol 2015; 33: 510–17.
Hong S, Beja-Glasser VF, Nfonoyim BM, Frouin A, Li S, Ramakrishnan S, et al. Complement and microglia mediate early synapse loss in Alzheimer mouse models. Science 2016; 352: 712–16.
Huisman C, Wisman GBA, Kazemier HG, van Vugt MATM, van der Zee AGJ, Schuuring E, et al. Functional validation of putative tumor suppressor gene C13ORF18 in cervical cancer by artificial transcription factors. Mol Oncol 2013; 7: 669–79.
Jain S, Yoon SY, Zhu L, Brodbeck J, Dai J, Walker D, et al. Arf4 determines dentate gyrus-mediated pattern separation by regulating dendritic spine development. PLoS One 2012; 7: e46340.
Jiang C, Pugh BF. Nucleosome positioning and gene regulation: advances through genomics. Nat Rev Genet 2009; 10: 161–72.
Kanasty RL, Whitehead KA, Vegas AJ, Anderson DG. Action and reaction: the biological response to siRNA and its delivery vehicles. Mol Ther 2012; 20: 513–24.
Konermann S, Brigham MD, Trevino AE, Hsu PD, Heidenreich M, Cong L, et al. Optical control of mammalian endogenous transcription and epigenetic states. Nature 2013; 500: 472–6.
Kungulovski G, Nunna S, Thomas M, Zanger UM, Reinhardt R, Jeltsch A. Targeted epigenome editing of an endogenous locus with chromatin modifiers is not stably maintained. Epigenetics Chromatin 2015; 8: 12.
Laganiere J, Kells AP, Lai JT, Guschin D, Paschon DE, Meng X, et al. An engineered zinc finger protein activator of the endogenous glial cell line-derived neurotrophic factor gene provides functional neuroprotection in a rat model of parkinson's disease. J Neurosci 2010; 30: 16469–74.
Langmead B, Salzberg SL. Fast gapped-read alignment with Bowtie 2. Nat Methods 2012; 9: 357–9.
Long C, Amoasii L, Mireault AA, McAnally JR, Li H, Sanchez-Ortiz E, et al. Postnatal genome editing partially restores dystrophin expression in a mouse model of muscular dystrophy. Science 2016; 351: 400–3.
Losi G, Prybylowski K, Fu Z, Luo J, Wenthold RJ, Vicini S. PSD-95 regulates NMDA receptors in developing cerebellar granule neurons of the rat. J Physiol 2003; 548: 21–9.
Mandell JG, Barbas CF. Zinc Finger Tools: custom DNA-binding domains for transcription factors and nucleases. Nucleic Acids Res 2006; 34: W516–23.

Mendenhall EM, Williamson KE, Reyon D, Zou JY, Ram O, Joung JK, et al. Locus-specific editing of histone modifications at endogenous enhancers. Nat Biotechnol 2013; 31: 1133–6.

Mingozzi F, High KA. Immune responses to AAV vectors: overcoming barriers to successful gene therapy. Blood 2013; 122: 23–36.

Myme CIO, Sugino K, Turrigiano GG, Nelson SB. The NMDA-to-AMPA ratio at synapses onto layer 2/3 pyramidal neurons is conserved across prefrontal and visual cortices. J Neurophysiol 2003; 90: 771–9.

Nelson CE, Hakim CH, Ousterout DG, Thakore PI, Moreb EA, Castellanos Rivera RM, et al. *In vivo* genome editing improves muscle function in a mouse model of Duchenne muscular dystrophy. Science 2016; 351: 403–7.

Neve RL, Neve KA, Nestler EJ, Carlezon WA. Use of herpes virus amplicon vectors to study brain disorders. Biotechnology 2005; 39: 381–91.

Roadmap Epigenomics Consortium, Heravi-Moussavi A, Wang J, Ziller MJ, Whitaker JW, Ward LD, et al. Integrative analysis of 111 reference human epigenomes. Nature 2015; 518: 317–30.

Savioz A, Leuba G, Vallet PG. A framework to understand the variations of PSD-95 expression in brain ageing and in Alzheimer's disease. Ageing Res Rev 2014; 18: 86–94.

Schlüter OM, Xu W, Malenka RC. Alternative N-terminal domains of PSD-95 and SAP97 govern activity-dependent regulation of synaptic AMPA receptor function. Neuron 2006; 51: 99–111.

Serrano FG, Tapia-Rojas C, Carvajal FJ, Hancke J, Cerpa W, Inestrosa NC. Andrographolide reduces cognitive impairment in young and mature AβPPswe/PS-1 mice. Mol Neurodegener 2014; 9: 61.

Shankar SR, Bahirvani AG, Rao VK, Bharathy N, Ow JR, Taneja R. G9a, a multipotent regulator of gene expression. Epigenetics 2013; 8: 16–22.

Smith ZD, Meissner A. DNA methylation: roles in mammalian development. Nat Rev Genet 2013; 14: 204–20.

Stolzenburg S, Beltran AS, Swift-Scanlan T, Rivenbark AG, Rashwan R, Blancafort P. Stable oncogenic silencing in vivo by programmable and targeted de novo DNA methylation in breast cancer. Oncogene 2015; 34: 5427–35.

Stricker SH, Köferle A, Beck S. From profiles to function in epigenomics. Nat Rev Genet 2017; 18: 51–66.

Sweatt JD. The emerging field of neuroepigenetics. Neuron 2013; 80: 624–32.

Tabebordbar M, Zhu K, Cheng JKW, Chew WL, Widrick JJ, Yan WX, et al. *In vivo* gene editing in dystrophic mouse muscle and muscle stem cells. Science 2016; 351: 407–11.

Tashiro A, Sandler VM, Toni N, Zhao C, Gage FH. NMDA-receptor-mediated, cell-specific integration of new neurons in adult dentate gyrus. Nature 2006; 442: 929–33.

van Zundert B, Peuscher MH, Hynynen M, Chen A, Neve RL, Brown RH, et al. Neonatal neuronal circuitry shows hyperexcitable disturbance in a mouse model of the adult-onset neurodegenerative disease amyotrophic lateral sclerosis. J Neurosci 2008; 28: 10864–74.

van Zundert B, Yoshii A, Constantine-Paton M. Receptor compartmentalization and trafficking at glutamate synapses: a developmental proposal. Trends Neurosci 2004; 27: 428–37.

Vargas JY, Fuenzalida M, Inestrosa NC. *In vivo* activation of Wnt signaling pathway enhances cognitive function of adult mice and reverses cognitive deficits in an Alzheimer's disease model. J Neurosci 2014; 34: 2191–202.

Voigt P, Reinberg D. Epigenome editing. Nat Biotechnol 2013; 31: 1097–9.

West AE, Chen WG, Dalva MB, Dolmetsch RE, Kornhauser JM, Shaywitz AJ, et al. Calcium regulation of neuronal gene expression. Proc Natl Acad Sci USA 2001; 98: 11024–31.

West AE, Greenberg ME. Neuronal activity-regulated gene transcription in synapse development and cognitive function. Cold Spring Harb Perspect Biol 2011; 3: a005744.

Zhang J, Saur T, Duke AN, Grant SGN, Platt DM, Rowlett JK, et al. Motor impairments, striatal degeneration, and altered dopamine-glutamate interplay in mice lacking PSD-95. J Neurogenet 2014; 28: 98–111.

Zhang LF, Ding JH, Yang BZ, He GC, Roe C. Characterization of the bidirectional promoter region between the human genes encoding VLCAD and PSD-95. Genomics 2003; 82: 660–8.